Nanowires of molecule-based charge-transfer salts†

Jean-Philippe Savy,[a] Dominique de Caro,*[a] Christophe Faulmann,[a] Lydie Valade,[a] Manuel Almeida,[b] Tadahiro Koike,[cd] Hideki Fujiwara,[cd] Toyonari Sugimoto,[cd] Jordi Fraxedas,[e] Thierry Ondarçuhu[f] and Claude Pasquier[gh]

Received (in Montpellier, France) 13th December 2006, Accepted 15th February 2007
First published as an Advance Article on the web 6th March 2007
DOI: 10.1039/b618241k

Nanowires of molecule-based charge-transfer salts are prepared using two different processing techniques. Isolated [TTF][TCNQ] nanowires are grown by a simple adsorption in organic solution method on stainless steel conversion coatings, used as substrates. They are characterized by Raman spectroscopy and current–voltage measurements. Nanowire films of $Per_2[Au(mnt)_2]$ and $(EDT\text{-}TTFVO)_4(FeCl_4)_2$ are electrodeposited on (001)-oriented silicon wafers, used as anodes. In the second case, growth as nanowires occurs after functionalizing the Si electrode with a phospholipidic membrane. Electrodeposited nanowire films are studied by various techniques, including electron microscopy, vibrational spectroscopies, X-ray photoelectron spectroscopy and conductivity measurements.

Introduction

Molecular materials containing organic or metal–organic components exhibit a variety of interesting properties, including electrical conductivity, magnetism, and non-linear optical properties.[1] Molecule-based materials are commonly prepared and studied as single crystals, a morphology in which they remain hardly integrable to devices. We have recently developed an electrolytic route to the formation of thin films of molecule-based conductors on silicon wafers used as substrates.[2] Thin-film morphology depends on the nature of the electrodeposited charge-transfer complex and on experimental conditions. Micrometer-sized roughly spherical grains, stacked sheets, or faceted microcrystals are usually observed.

Nanometer scale molecule-based materials have received broad attention in recent years because of their novel properties and potential applications. However, nanoclusters and nanowires of molecular conductors are still rare, and only few examples have been reported. For instance, nanoclusters of [TTF][TCNQ] evaporated on Au(111)[3] and nanocrystallites of [TTF]Br grown on platinum nanoparticles[4] have been described (TTF: tetrathiafulvalene; TCNQ: tetracyanoquinodimethane, Scheme 1). Moreover, nanowires of neutral tetrathiafulvalene-based derivatives and of charge-transfer complexes can be fabricated by a dipping method using a Langmuir trough,[5] a drop casting technique,[6] adsorption in organic solution,[7] galvanostatic electrochemical deposition method using porous aluminium oxide as template,[8] or thermal evaporation under a high electric field.[9] This latter technique leads to oriented individual [TTF][TCNQ] nanowires but require a sophisticated apparatus. Moreover, the precursor materials must be sublimed and transported without any decomposition from the crucibles to the deposition zone. This is the case for TTF and TCNQ but usually not the case when ionic coordination complexes are involved.

We describe in this paper the facile and reproducible preparation of nanowires of charge-transfer salt-based conductors on various substrates (stainless steel conversion coatings, silicon wafers and silicon-supported multilamellar membranes) by adsorption technique ([TTF][TCNQ]) or by galvanostatic electrochemical deposition ($Per_2[Au(mnt)_2]$ and $(EDT\text{-}TTFVO)_4(FeCl_4)_2$, where Per: perylene; mnt^{2-}: maleonitriledithiolate (Scheme 2); EDT-TTFVO: ethylenedithiotetrathiafulvalenoquinone-1,3-dithiolemethide (Scheme 3)).

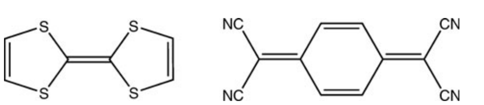

Scheme 1 Molecular structures of TTF and TCNQ.

[a] *Laboratoire de Chimie de Coordination (CNRS UPR 8241), 205, route de Narbonne, F-31077 Toulouse Cedex 4, France. E-mail: decaro@lcc-toulouse.fr; Fax: +33 (0)5-61-55-30-03 Tel: +33 (0)5-61-33-31-06*
[b] *Departamento de Química, Instituto Tecnológico Nuclear/CFMC Estrada National no. 10, P-2685-953 Sacavém, Portugal. E-mail: malmeida@itn.pt; Fax: +351 219941455*
[c] *Department of Chemistry, Graduate School of Science, Osaka Prefecture University, Osaka, 599-8570, Japan*
[d] *CREST, Japan Science and Technology Agency, Saitama, 332-0012, Japan. E-mail: toyonari@c.s.osakafu-u.ac.jp; Fax: +81 72 252 4175*
[e] *Institut de Ciència de Materials de Barcelona (CSIC), Campus de la UAB, E-08193 Bellaterra, Spain. E-mail: fraxedas@icmab.es Fax: +34 93-5805729*
[f] *Centre d'Elaboration de Matériaux et d'Etudes Structurales (CNRS UPR 8011), 29, rue Jeanne Marvig, BP 4347, F-31055 Toulouse Cedex 4, France. E-mail: Thierry.Ondarcuhu@cemes.fr Fax: +33 (0)5-62-25-79-99*
[g] *Laboratoire de Physique des Solides, Université Paris-Sud, UMR 8502, F-91405 Orsay, France. E-mail: pasquier@lps.u-psud.fr Fax: +33 (0)1-69-15-60-86*
[h] *CNRS, F-91405 Orsay, France*

† Electronic supplementary information (ESI) available: Large SEM view of [TTF][TCNQ] nanowires and elongated platelets, IR spectrum for $Per_2[Au(mnt)_2]$, Raman spectrum for $Per_2[Au(mnt)_2]$, stacking arrangement and overlapping modes of EDT-TTFVO donors in $(EDT\text{-}TTFVO)_4(FeCl_4)_2$, Raman spectrum for Si-supported multilamellar membranes. See DOI: 10.1039/b618241k

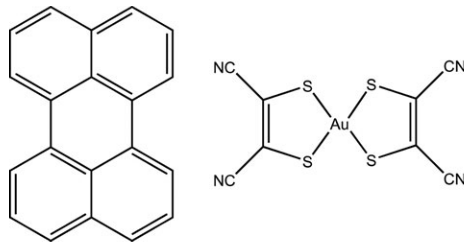

Scheme 2 Molecular structures of perylene and $Au(mnt)_2$.

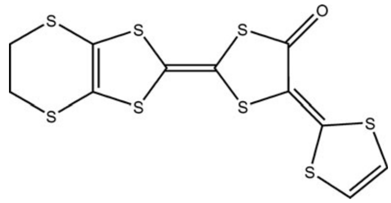

Scheme 3 Molecular structure of EDT-TTFVO.

Experimental

Chemicals

TTF, TCNQ, perylene, and $DC_{8,9}PC$ [1,2-bis(10,12-tricosadiynoyl)-*sn*-glycero-3-phosphocholine] are commercially available and used without further purification. Solvents were freshly distilled and degassed under argon before use.

Substrates

The stainless steel conversion coatings were prepared from austenitic stainless steel sheets (0.5×0.5 cm^2; 0.01 wt% Al, 0.03 wt% C, 17.4 wt% Cr, 0.13 wt% Cu, 1.78 wt% Mn, 0.15 wt% Mo, 9.41 wt% Ni, 0.45 wt% Si, 0.07 wt% V) dipped in a sulfuric acid bath (0.2% by volume) containing sodium thiosulfate (0.01 mol L^{-1}) at 55 °C. After an electrolytic activation (−1.5 V *vs.* SCE) for 2 min, the conversion coating was grown by chemical treatment in the same bath for 20 min. The sample was then washed with water and dried at 75 °C for 60 min before use.

Intrinsic silicon wafers were purchased from Siltronix (diameter: 5 cm; thickness: 275 μm; resistivity at room temperature: about 200 Ω cm). Electrodepositions of $Per_2[Au(mnt)_2]$ nanowires and $(EDT\text{-}TTFVO)_4(FeCl_4)_2$ single crystals were carried out on a silicon wafer prepared as follows: pieces of wafers (rectangular shape: 0.5×1 cm^2) were cleaned ultrasonically in acetone for 3 min. They were dipped in a mixture of H_2SO_4–H_2O_2 (1 : 1 v/v) for 10 min and rinsed with water (30 s). They were then dipped in a mixture of H_2O–HF (9 : 1 v/v) for 10 min and rinsed with water (30 s). They were finally dipped in a mixture of H_2SO_4–H_2O_2 (1 : 1 v/v) for 10 min and rinsed with dichloromethane for 10 min ($Per_2[Au(mnt)_2]$) or with chlorobenzene–ethanol (9 : 1 v/v). Electrodeposition of $(EDT\text{-}TTFVO)_4(FeCl_4)_2$ nanowires was performed on hydrophilic silicon-supported multilamellar membranes prepared according to the method described before.[10]

Nanowire film preparation

All the nanowire films obtained are stable to air and moisture.

[TTF][TCNQ]. The nanowire formation was carried out inside a glove-box filled with argon. The stainless steel conversion coating was dipped in a beaker containing an acetonitrile solution of TTF (0.01 mol L^{-1}). Adsorption of the donor molecule was realized under slow stirring for 30 min. The substrate was then dried for 1 min and dipped in a second beaker containing an acetonitrile solution of TCNQ (0.01 mol L^{-1}). Reaction with TTF was realized under slow stirring for 30 min. The [TTF][TCNQ]-containing stainless steel conversion coating was finally dried under argon for 10 min.

$Per_2[Au(mnt)_2]$. A solution of perylene (35 mg) and $[(n\text{-}C_4H_9)_4N][Au(mnt)_2]$ (25 mg) in CH_2Cl_2 (12 mL) was introduced into the anodic compartment of an H-type electrochemical cell (anode: Si). A solution of $[(n\text{-}C_4H_9)_4N][Au(mnt)_2]$ (25 mg) in CH_2Cl_2 (12 mL) was introduced into the cathodic compartment where it only acts as supporting electrolyte (cathode: Pt wire). The oxidation of the perylene organic donor was performed at constant current density (0.30 μA cm^{-2}) at room temperature in the presence of $[(n\text{-}C_4H_9)_4N][Au(mnt)_2]$. Within 3 days, a black deposit (thickness ∼10 μm) was obtained on the silicon anode.

$(EDT\text{-}TTFVO)_4(FeCl_4)_2$

Single crystals. A solution of EDT-TTFVO (10 mg) and $[(n\text{-}C_2H_5)_4N]FeCl_4$ (100 mg) in 30 mL of a mixture of chlorobenzene–ethanol (9 : 1 v/v) was electrocrystallized at 0.15 μA cm^{-2} for 10 days at 25 °C (cathode: Pt wire; anode: Si wafer).

Nanowire films. A solution of EDT-TTFVO (5 mg) and $[(n\text{-}C_2H_5)_4N]FeCl_4$ (50 mg) in 15 mL of a mixture of chlorobenzene–ethanol (9 : 1 v/v) was introduced into the anodic compartment of an H-type electrochemical cell (anode: Si-supported multilamellar membrane). A solution of $[(n\text{-}C_2H_5)_4N]FeCl_4$ (100 mg) in 15 mL of a mixture of chlorobenzene–ethanol (9 : 1 v/v) was introduced into the cathodic compartment where served as supporting electrolyte (cathode: Pt wire). The oxidation of the EDT-TTFVO organic donor was performed at constant current density (0.15 μA cm^{-2}) at room temperature in the presence of the $FeCl_4^-$ anion. Within 10 days, a very thin black deposit (visible using an optical microscope) was obtained on the silicon-supported multilamellar membrane.

Characterization techniques

Elemental analyses were performed by the Microanalysis Service of LCC-CNRS.

Scanning electron micrographs of [TTF][TCNQ] nanowires were obtained on a Jeol Model JSM 840A microscope. Scanning electron micrographs of $Per_2[Au(mnt)_2]$ and $(EDT\text{-}TTFVO)_4(FeCl_4)_2$ nanowires were obtained on a JEOL JSM 6700F scanning electron microscope equipped with a field-effect gun.

Infrared spectra of $Per_2[Au(mnt)_2]$ were recorded (in KBr matrix) on a sample of the film peeled off from the silicon surface, using a Perkin-Elmer Spectrum GX spectrophotometer.

Raman measurements were performed using a LabRAM-HR800 (Jobin Yvon) set-up. The spectra were obtained at room temperature using the 632.8 nm line of an He–Ne laser.

The incident beam was focused onto the deposit through the $\times100$ optical microscope objective, giving a spot size of $\sim1\ \mu m^2$. The back-scattered light was collected through the same objective, dispersed (single-grating spectrograph, 1800 grooves mm^{-1}, f = 80 cm) and then imaged onto a CCD detector (Andor DU420-OE). Using a laser power density of about 1.7×10^6 W cm^{-2}, no degradation of the material was observed.

X-Ray diffraction data for $Per_2[Au(mnt)_2]$ nanowire films were collected using a home-made diffractometer (Sacavém facility working with Cu-Kα radiation at 1.5418 Å), either in $\theta/2\theta$ configuration or in grazing angle configuration ($\theta = 4°$). X-Ray photoelectron spectroscopy (XPS) data were acquired with an EA10P hemispherical analyser (SPECS) using non-monochromatized Mg-Kα radiation (1253.6 eV, 300 W). The samples were held at room temperature at a base pressure of $\sim10^{-9}$ mbar.

The conduction properties of [TTF][TCNQ] nanowires were evaluated at room temperature by plotting their current–voltage (I–V) response when placed between two electrodes of a metal–insulator–metal nanojunction fabricated on a silica surface as previously described.[11] Conductivity measurements of $Per_2[Au(mnt)_2]$ nanowire films were performed using the standard four-probe method. Electrical contacts between the gold wires and the film were made by using gold paint. They were drawn parallel to each other keeping a large inter-wire distance (1.75 mm).

Crystal data for $(EDT\text{-}TTFVO)_4(FeCl_4)_2$

$C_{22}H_{12}Cl_4FeO_2S_{16}$, M = 1018.93, T = 113(2) K, monoclinic, $P2_1/c$, a = 14.2714(9), b = 12.8482(10), c = 39.425(3) Å, β = 104.958(7)°, V = 6984.0(9) Å^3, Z = 8, D_c = 1.938 Mg m^{-3}, μ = 1.723 mm^{-1}, R = 0.1042, w$R2$ = 0.2612.

CCDC reference number 627188. For crystallographic data in CIF or other electronic format see DOI: 10.1039/b618241k

Results and discussion

[TTF][TCNQ] nanowires on stainless steel conversion coatings

[TTF][TCNQ] is the most representative organic conductor. This charge-transfer salt exhibits a crystalline structure composed of parallel chains of both donors (TTF) and acceptors (TCNQ) molecules. This salt shows a highly anisotropic electrical conductivity ($\sigma_b \sim 600$ S cm^{-1}; $\sigma_b/\sigma_a \sim 10^3$). It exhibits three Peierls transitions at 54, 49 and 38 K, due to successive removal of the metallic conductivity along the TCNQ and the TTF chains. This organic metal has undoubtedly been the most processed as thin films, namely by molecular beam deposition,[12] chemical vapour deposition,[13] and thermal sublimation in high vacuum.[14] A recent study reports the fabrication of [TTF][TCNQ] nanowires by a co-evaporation technique with an applied electric field.[9] By optimization of applied voltage and reduction of electrode gap, the authors could prepare nanowires connecting the gold anode and the gold cathode. The almost linear I–V curve (in the [−1; +1] V range) indicates the ohmic junction between the Au electrode and [TTF][TCNQ] wire. Moreover, a semiconductor-like conduction is shown by the temperature dependence of the conductivity.[9] However, this technique, although leading to very interesting results, requires a quite sophisticated experimental set-up.

We have recently developed an easier route to [TTF][TCNQ] nanowires by an adsorption in organic solution method utilizing a stainless steel conversion coating as substrate.[15] Stainless steel conversion coatings have been known for showing advanced adsorption properties due to their nanostructured surface and have been applied to fix dyes[16] or to improve the adherence of further coatings.[17] [TTF][TCNQ] nanowires are prepared by successive immersion of the stainless steel conversion coating in acetonitrile solutions of TTF and TCNQ. Adsorption of TTF is realized at first. Then, immersion of the TTF-containing oxide surface in the TCNQ solution results in the formation of [TTF][TCNQ] nanowires together with a few platelets. Nanowires uniformly cover the substrate surface and a large amount of them bridge the cracks of the conversion coating (Fig. 1). Efficient adsorption of the TTF moiety onto the surface is not surprising because stainless steel conversion coatings are known to adsorb large planar azo dyes.[16] Further formation of [TTF][TCNQ] as nanowires and not as a continuous film could be explained by the 1D-character of the charge-transfer salt, as previously reported for CuTCNQ or AgTCNQ nanowires grown on metal foils exposed to TCNQ vapors.[18]

In our previous paper,[15] charge transfer investigations using Raman spectroscopy and detailed transport properties were not carried out. We report here the Raman data and further conducting properties. In the 1400–1600 cm^{-1} range, the Raman spectrum (recorded on an elongated platelet) exhibits three lines, all related to C=C modes (Fig. 2). The first line, exhibiting two maxima at 1413 and 1418 cm^{-1}, corresponds to the ν_4 a_g mode in TCNQ. Using the linear relation of the TCNQ ν_4 frequency *vs.* ρ (amount of charge transfer) established by Matsuzaki *et al.*,[19] we determine a degree of charge transfer ranging from 0.65 to 0.60, in good agreement with the value of 0.59 for single crystals. The second line (1512 cm^{-1}) is due to the ν_2 a_g mode in TTF. Its position is intermediate between neutral TTF (1555 cm^{-1}) and TTF^+ (1505 cm^{-1}).[20] The third frequency (1600 cm^{-1}) is assigned to the ν_3 a_g mode in TCNQ, which is less sensitive to charge-transfer change (1602 cm^{-1} for neutral TCNQ and 1595 cm^{-1} for $TCNQ^-$).[21]

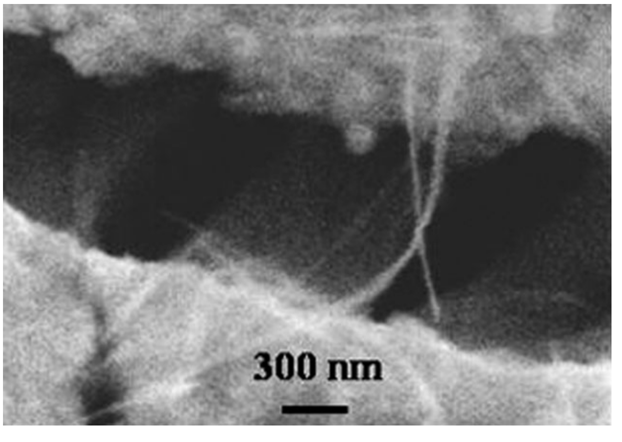

Fig. 1 SEM image of [TTF][TCNQ] nanowires.

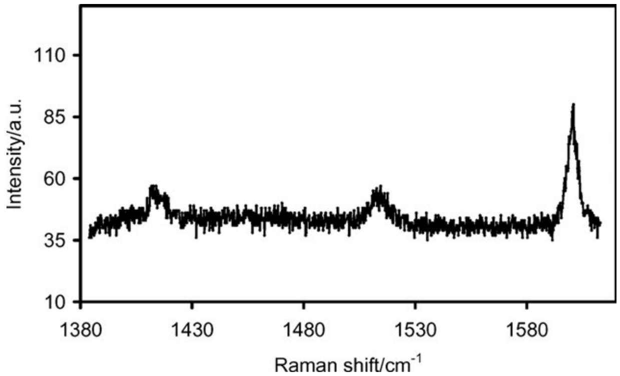

Fig. 2 Raman spectrum recorded on an elongated [TTF][TCNQ] platelet.

The [TTF][TCNQ] nanowires can be collected using a micropipette (diameter <1 μm) gently scanned with a micromanipulator inside the cracks of the conversion coating, and placed between two metallic electrodes separated by a gap of few nanometers fabricated on a Si/SiO_2 substrate. The *I–V* curve thus obtained is shown in Fig. 3. The non-linearity of the *I–V* curve might be attributed to the non-ohmic character of the contacts which is possibly due to an imperfect interface between the electrodes and the nanowire, in contrast with techniques where the sample grows directly from one electrode to the other.[9] The existence of a tunnel junction at the electrode–[TTF][TCNQ] nanowire junction is therefore highly possible. Indeed, the observed gap of about 0.3 eV is compatible with values obtained by scanning tunnelling spectroscopy[22] and photoemission measurements[23] performed on [TTF][TCNQ] single crystals.

$Per_2[Au(mnt)_2]$ nanowires on silicon wafers

After [TTF][TCNQ], conductors based on transition-metal complexes with bis(dithiolate) ligands are the most intensively studied as thin films. For instance, $(TTF)[Ni(dmit)_2]_2$ ($dmit^{2-}$: 2-thioxo-1,3-dithiol-4,5-dithiolato),[24] $[(n\text{-}C_4H_9)_4N]_2[Ni(dcbdt)_2]_5$ ($dcbdt^{2-}$: 4,5-dicyanobenzene-1,2-dithiolato),[25] (BEDT-TTF)$[Ni(dcbdt)_2]$ (BEDT-TTF: bis(etylenedithio)tetrathiafulvalene),[25] (BEDT-TTF)$[Ni(dmit)_2]_2$,[26] and $Ni(tmdt)_2$ ($tmdt^{2-}$: trimethylenetetrathiafulvalenedithiolate)[27] have been processed as thin films on an intrinsic (001)-oriented Si wafer

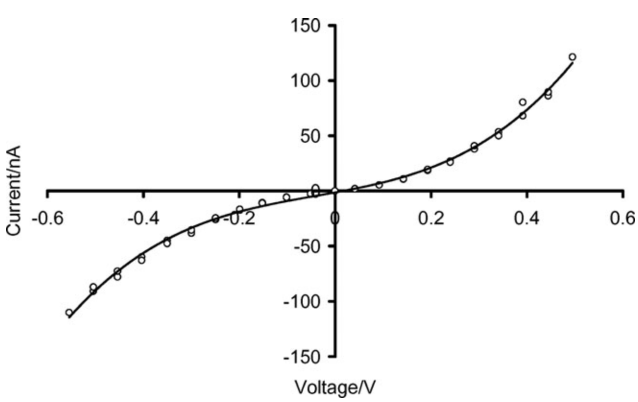

Fig. 3 *I–V* curve on [TTF][TCNQ] nanowires.

used as an anode in a common electrocrystallization process. Roughly spherical micrograins, thin microplatelets, faceted microcrystals, and flower-like microcrystals are, respectively, observed.

The Langmuir–Blodgett (LB) technique is another way to organize bis(dithiolate)-based materials on surfaces. Typically, in a first step, LB-films of $mC_nM(dmit)_2$ are prepared (M = Ni, Au, $mC_n = (C_nH_{2n+1})_mN(CH_3)_{4-m}$ where n = 10, 14, 16, 18 and m = 2 or 3).[28] In a second step, gold electrodes are evaporated on the films and used for electrochemical oxidation of the 1 : 1 Langmuir–Blodgett salts.

We then decided to focus our attention on another series of charge transfer salts based on transition-metal complexes bearing bis(dithiolate) ligands, namely $Per_2[M(mnt)_2]$. Their interest resides upon the coexistence in the same system of delocalized electron chains (perylene molecules) and chains of localized spins ($M(mnt)_2^-$ units).[29] α-$Per_2[M(mnt)_2]$ (M = Fe, Co, Ni, Pd, Pt, Cu, Au) phases have a very similar structure, with segregated stacks of perylene and $M(mnt)_2$ units along the *b* direction. They present at high temperatures a metallic regime of the electrical conductivity measured along the stacking axis (*b*), and undergo metal-to-insulator transitions at lower temperatures. At room temperature, the electrical conductivity was found to be of the order of 700 S cm^{-1} for the M = Ni, Pt, Cu, Au compounds, 300 S cm^{-1} for M = Pd, and 200 S cm^{-1} for the M = Fe and Co compounds.

The magnetic behaviour of these compounds is strongly dependent on the metal. For diamagnetic $M(mnt)_2^-$ moieties (M = Co, Cu, Au), the magnetic susceptibility is due only to a small contribution of the perylene conduction electrons, which vanishes at the metal-to-insulator transition. A much larger magnetic susceptibility, due to an additional contribution of a chain of localized spins on the anions, is observed in cases of paramagnetic $M(mnt)_2^-$ units. β-$Per_2[M(mnt)_2]$ phases are well known for M = Ni and Cu (semiconducting behaviour clearly distinct from the metal-like high-temperature regime of the α-phases). Although not confirmed by X-ray diffraction, they probably exist also in other cases, such as M = Au, where transport and magnetic studies provide similar evidence for the existence of the β-phase.

Though diamagnetic, we have chosen $Au(mnt)_2^-$ (Au^{3+} square planar d^8 configuration) to study its association with perylene molecules on a silicon wafer as anode, for the following reasons:

(i) its high room-temperature conductivity value (when growing as the α-phase),

(ii) its Peierls transition to a charge density wave ground state, where clear non-linear electrical transport properties are observed,[30,31]

(iii) the presence of a relatively intense Au 4f line (in the X-ray photoelectron spectrum) whose position is very sensitive towards the formal oxidation number of the gold centre and towards electronic delocalization through dithiolate ligands.

Electrodeposition at constant current density from perylene and $[(n\text{-}C_4H_9)_4N][Au(mnt)_2]$ in dichloromethane at room temperature on an intrinsic (001)-Si anode leads to a black film uniformly covering the silicon surface. Elemental analysis of a sample of film scratched from the surface gives the following result: C, 58.23; H, 2.28; N, 5.70%. These values are in good

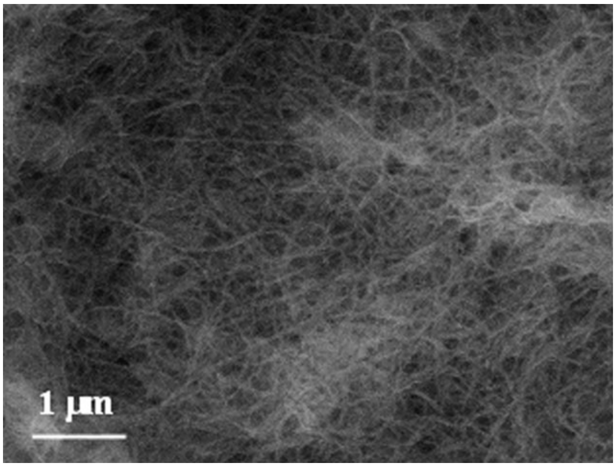

Fig. 4 SEM image of $Per_2[Au(mnt)_2]$ nanowire films.

agreement with the data calculated for $Per_2[Au(mnt)_2]$, *i.e.* $C_{48}H_{24}N_4S_4Au$ (C, 58.78; H, 1.22; N, 5.70%). Therefore, the same 2 : 1 stoichiometry as that of $Per_2[Au(mnt)_2]$ single crystals can be postulated for the films.

Scanning electron micrographs reveal that the film coated on the surface of silicon surprisingly consists of large-scale $Per_2[Au(mnt)_2]$ nanowires (Fig. 4). The diameter of an individual nanowire is in the narrow range of 35–55 nm. Typical film thicknesses are about 10 µm, which are evaluated from the side view of the sample.

Vibrational data confirm the presence of both perylene and $Au(mnt)_2$ units. The Raman spectrum is dominated by the C=C stretching modes for both the perylene molecules and the dithiolate ligands (in the 1250–1750 cm^{-1} range). Low frequency bands at 370, 528 and 800 cm^{-1} (which are not present in the Raman spectrum of perylene) could be assigned to the Au–S stretching mode, AuS_2C_2 ring deformation mode, and C–S stretching mode, respectively.[32,33] The infrared spectrum evidences CH ethylenic stretching modes for perylene (3046 cm^{-1}) and CN stretching modes for the nitrile groups of mnt^{2-} ligands (2208 and 2220 cm^{-1}).

Although molecule-based conductors have been grown as thin films on non-functionalized semiconducting[24–27] or metallic electrodes (Pt,[34] Au[35]), or on metallic electrodes (Cu) in the presence of a poly counter cation,[36] to our knowledge, this is the first time that such electrochemically-grown films exhibit a nanowire-like morphology. The mechanism of nanowire formation is not yet understood. However, we have very recently shown that TMTSF-based conductors could be electrochemically processed as thin films consisting of microneedles ($(TMTSF)_2ClO_4$),[37] or of microwires ($(TMTSF)_5[Co(dcbdt)_2]_4$),[38] uniformly covering the silicon surface (TMTSF: tetramethyltetraselenafulvalene).

Fig. 5(a) and (b) show the Au 4f and N 1s XPS lines, respectively, measured on a $Per_2[Au(mnt)_2]$ thin film. The binding energy of the Au $4f_{7/2}$ peak is 86.1 eV, which can be associated to a formal Au(III) oxidation state.[39] The shape of the lines (essentially symmetric) together with their small full width at half maximum (FWHM), 0.8 eV, strongly suggest that the dominant contribution corresponds to Au(III) and that other non-zero oxidation states of gold contribute negligibly to the signal, *i.e.*, absence of mixed-valency. Around 84 eV binding energy, a small contribution from metallic gold is detected, which may arise from gold nanoparticles or aggregates within the films. Their formation may be induced by the incident X-ray beam.

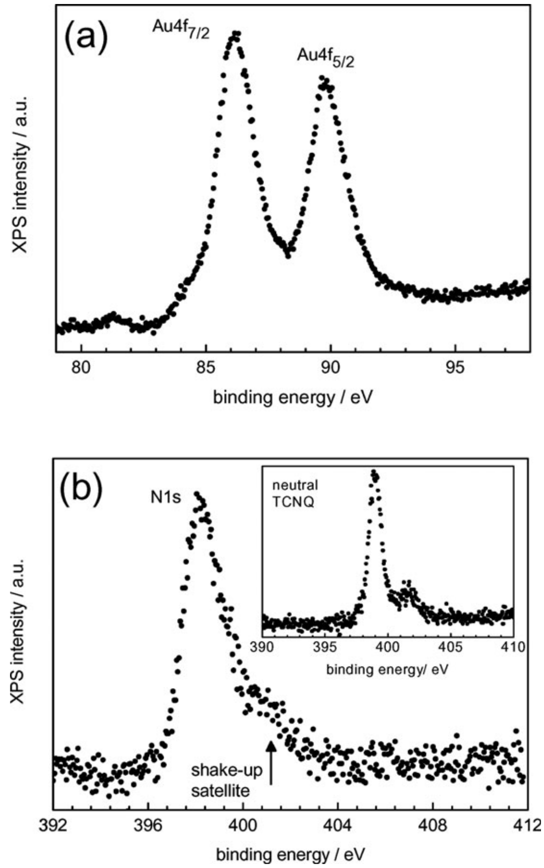

Fig. 5 XPS Au 4f (a) and N 1s (b) lines measured at room temperature of a $Per_2[Au(mnt)_2]$ nanowire film (inset: N 1s line of neutral TCNQ).

The N 1s line (Fig. 5(b)) is composed of a main peak located at 398.2 eV binding energy and a shoulder at *ca.* 401 eV. The lineshape is characteristic of the presence of the cyano group, with a main peak and a (shake-up) satellite. The satellite arises from the energy loss (about 3 eV) of electrons associated to the occupied–unoccupied CN-related states, a known feature previously evidenced in neutral TCNQ: the inset of Fig. 5(b) shows the XPS spectrum of the N 1s line of neutral TCNQ taken at high resolution in which the observation of the satellite is more evident. XPS spectra taken on $[(n\text{-}C_4H_9)_4N][Au(mnt)_2]$ pressed pellets (not shown) give binding energies for Au $4f_{7/2}$ and N 1s of 86.3 and 398.4 eV, respectively, thus close to the values obtained for $Per_2[Au(mnt)_2]$. In this case the CN-related satellite is masked by the presence of a peak located at 401.5 eV, which corresponds to the nitrogen from $(n\text{-}C_4H_9)_4N^+$.[25]

X-Ray diffraction studies evidence that the films have an amorphous or nanocrystalline character, this latter observation being in agreement with the observation of nanowires.

The electrical conductivity of $Per_2[Au(mnt)_2]$ nanowire films is about 0.02 S cm^{-1} at room temperature and follows a

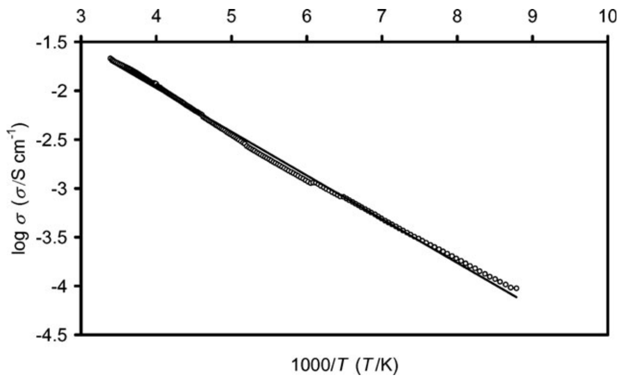

Fig. 6 Conductivity as a function of reciprocal temperature for electrodeposited $Per_2[Au(mnt)]_2$ nanowire films.

thermally activated semiconducting behaviour. The plot of log(σ) *vs.* $1/T$ shows an activation energy of 88 meV in the 100–298 K range (Fig. 6). Below 100 K, the resistance of the sample was too large to be measured with our facility. The room-temperature conductivity of the film is about 10^4 times lower than that of single crystals.[29] Within single crystals, the stacking axis b is the direction of highest conductivity. The contributions of other directions due to random orientation of the nanowires on the surface, and presence of inter-nanowire contacts which are presumably more resistive than the material itself, account for the lower conductivity value of the film *vs.* that of single crystals.

$(EDT\text{-}TTFVO)_4(FeCl_4)_2$ nanowires on silicon-supported multilamellar membranes

Symmetrical and unsymmetrical tetrathiafulvalene- or tetraselenafulvalene-based donors associated to FeX_4^- or GaX_4^- anions (X = Cl, Br) are of great interest. For example, a number of BETS-based conductors with the so-called θ-, λ- and κ-type molecular arrangements have been prepared [BETS: bis(ethylenedithio)tetraselenafulvalene]. They retain metallic behaviour down to low temperatures. In such π–d systems where the π electrons are conducting and the d spins are localized. The antiferromagnetic superconductor κ-$(BETS)_2FeBr_4$,[40,41] and the field-induced ferromagnetic superconductor λ-$(BETS)_2FeCl_4$, represent the most interesting examples.[42]

Recently, promising unsymmetrical donors associated to FeX_4^- or GaX_4^- anions have appeared.[43–47] Charge transfer salts combining ethylenedithiotetrathiafulvalenoquinone-1,3-dithiolemethide (EDT-TTFVO) with an $FeCl_4^-$ or $FeBr_4^-$ ion can be obtained using a two- or three-phase contact method.[43,44] The 2 : 1 salts thus obtained display crystal morphology-dependent physical properties. $(EDT\text{-}TTFVO)_2FeBr_4$ can be obtained either as plate crystals or as needle crystals. The plate crystals show a semiconducting behaviour (room-temperature conductivity: 15.5 S cm^{-1}; activation energy: 57 meV),[43] whereas the needle crystals exhibit a metallic conductivity (room-temperature conductivity: 4.6 S cm^{-1}) and ferromagnetic interactions of Fe^{III} d spins.[44] $(EDT\text{-}TTFVO)_2FeCl_4$ has been only described as plate crystals (prepared by contact between EDT-TTFVO in CS_2 and $FeCl_3$ in CH_3CN), exhibiting a room-temperature conductivity of 0.8 S cm^{-1} (measured in the wide plane) and a semiconducting behaviour (activation energy: 120 meV).[43] On the other hand, we have recently shown that a silicon electrode could induce the formation of $(BEDT\text{-}TTF)_2SbF_6$ with a crystal structure different from that obtained by a common platinum electrode or by a multi-phase slow diffusion technique.[26]

We then decided to perform electrocrystallization on a silicon wafer of EDT-TTFVO in the presence of $[(n\text{-}C_2H_5)_4N]FeCl_4$ as reactant and supporting electrolyte. We do not end up with a film but rather black single crystals randomly dispersed on the Si electrode. Scanning electron micrographs evidence that the single crystals resemble overlapping wood planks (size: 10–50 × 50–100 μm^2).

X-Ray structure determination (with C atoms isotropically refined) of a black plate-shaped crystal surprisingly shows that they are not the previously-obtained phase identified as $(EDT\text{-}TTFVO)_2FeCl_4$,[43] but a new crystal phase with the formula $(EDT\text{-}TTFVO)_4(FeCl_4)_2$ (Fig. 7). The main difference between these two phases lies in the stacking and overlapping modes of the EDT-TTFVO units (see Fig. S4 and S5 in ESI†). In $(EDT\text{-}TTFVO)_2FeCl_4$, the donors form regular columns, stacking either in a head-to-tail or in a head-to-head mode.[43] This results in a homogeneous network of S···S interactions (<3.80 Å). On the other hand, in $(EDT\text{-}TTFVO)_4(FeCl_4)_2$, all columns (along the a axis) are built on trimers and monomers. Successive donors always stack in a head-to-tail mode. There also exist several short S···S contacts (<3.80 Å) between donors of neighbouring stacks (along the b direction). This creates a 2D-network of S···S interactions but this is much less homogeneous than in the case of $(EDT\text{-}TTFVO)_2FeCl_4$.

This is in agreement with the electrical conductivity of $(EDT\text{-}TTFVO)_4(FeCl_4)_2$ which is lower than that of the plate-shape 2 : 1 phase. However, it should be noted that the

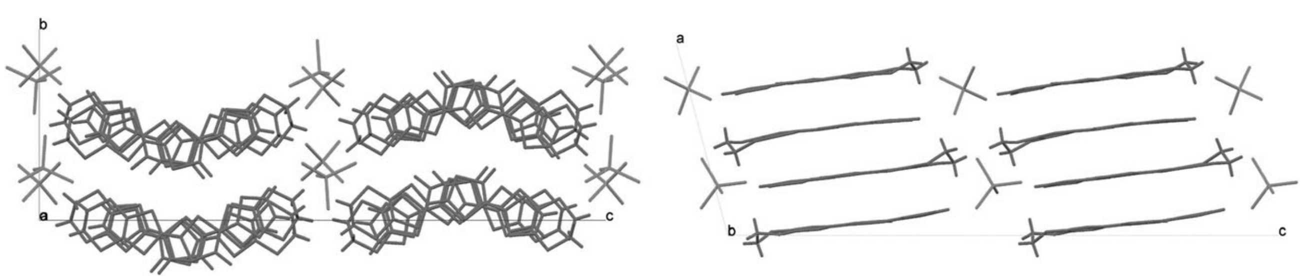

Fig. 7 View of the structure of $(EDT\text{-}TTFVO)_4(FeCl_4)_2$ along the a axis (right) and along the b axis (left).

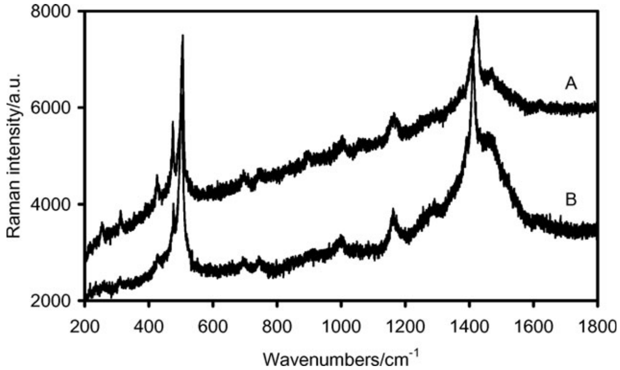

Fig. 8 Raman spectra of $(EDT\text{-}TTFVO)_4(FeCl_4)_2$ single crystals (A) and nanofibre films (B).

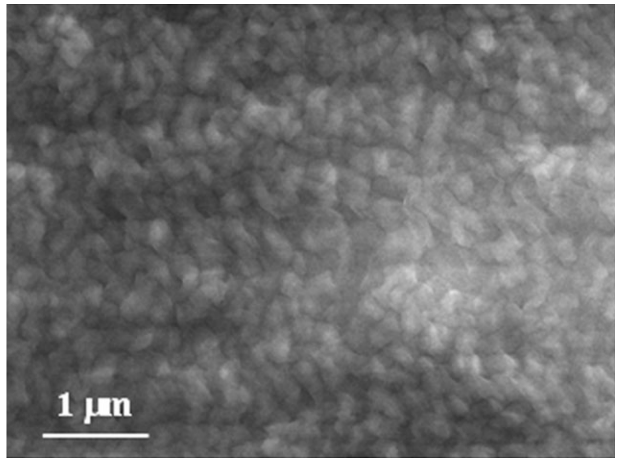

Fig. 9 Electron micrograph of $DC_{8,9}PC$ multilayers as methanol–chloroform solutions on (001)-oriented silicon wafers.

conductivity of $(EDT\text{-}TTFVO)_4(FeCl_4)_2$ single crystals is measured across the thickness of the plate-shaped crystal. The conductivity lies in the 10^{-3}–10^{-4} S cm^{-1} range and decreases when the temperature is lowered down to 77 K. However, the activation energy value for $(EDT\text{-}TTFVO)_4(FeCl_4)_2$ single crystals is about 35 meV, interestingly lower compared to that for $(EDT\text{-}TTFVO)_2FeCl_4$ single crystals (120 meV).[43] It has been impossible to measure the resistance in the plane of the crystal due to a non-ohmic behaviour.

The Raman spectrum of the single crystals (Fig. 8, spectrum A) exhibits a signal at 312w cm^{-1}, assigned to the ν_{Fe-Cl} a_1 mode, confirming the presence of the $FeCl_4^-$ ion.[48] The weak signal at 255 cm^{-1} is assigned to both δ_{S-C-S} and δ_{C-S-C} deformation modes, by comparison with literature data for TTF.[20] The two peaks located at 506s and 753w cm^{-1} can be attributed to ν_{C-S} modes involving C(sp^2) carbon atoms of the central TTF part and of the peripheral semi-TTF part of the EDT-TTFVO molecule.[20] The band at 1005w cm^{-1} corresponds to the ν_{C-C} stretching mode of the ethylenedithio group, by comparison with literature data for BEDT-TTF.[49] Signals at 1423s and 1471sh cm^{-1} are assigned to $\nu_{C=C}$ stretching modes. For the neutral EDT-TTFVO molecule, the corresponding bands are located at 1450s and 1504sh cm^{-1}. Lower C=C frequencies observed for $(EDT\text{-}TTFVO)_4(FeCl_4)_2$ single crystals are in agreement with the cationic character of the EDT-TTFVO molecule. Finally, the weak band at 1626 cm^{-1} is due to the carbonyl stretching mode.

In conclusion, we have shown the ability of an intrinsic silicon electrode to grow a new crystal phase combining EDT-TTFVO (formally +0.5) and $FeCl_4^-$ ion, distinct from that obtained by a purely chemical oxidation. As thin films of this new phase do not grow on neat silicon, we have decided to use a Si-supported multilemallar membrane as template, following a recently published procedure.[10]

This work reports a new approach for fabricating organic–inorganic superlattices by electrochemical deposition of nickel hydroxide into solid-supported multilamellar templates. The well-ordered multilamellar templates are produced by spreading small drops of lipid solution on Si surfaces and allowing the solvent to evaporate slowly. The templates which are used as working electrodes can preserve the lamellar structure in the electrolyte solution. The phospholipid used ($DC_{8,9}PC$) contains a zwitterion type headgroup and two long alkyl chains. Each alkyl chain has two conjugated carbon–carbon triple bonds which can polymerize by irradiation with UV light.[10] In ref. 10, the interheadgroup spacings are filled with nickel nitrate aqueous solution. Reduction reaction of NO_3^- to NO_2^- ions starts at the interface between the first bilayer and the silicon substrate. Electrochemically generated OH^- ions combine immediately with Ni^{2+} ions, and the resultant $Ni(OH)_2$ precipitates then fill the first interface. The growth front moves interface by interface until, finally, it reaches the topmost interface, producing a well defined lamellar nanostructure with nickel hydroxide layers intercalated between the lipid bilayers.

We have prepared Si-supported multilamellar membranes (thickness ~2.6 μm) according to the experimental procedure described in ref. 10. A drop of a CH_3OH–$CHCl_3$ solution of $DC_{8,9}PC$ was spread on the silicon substrate. After the solvent was allowed to slowly evaporate, the residue was irradiated with UV light. Membranes thus obtained have been characterized by scanning electron microscopy and by Raman spectroscopy. Surface profile images evidence that membranes are homogeneous (Fig. 9). These results are similar to those performed by AFM surface morphology analyses.[10] In the 1300–3050 cm^{-1} range, Raman spectra exhibit stretching (2893 cm^{-1}) and deformation (1455 cm^{-1}) modes of the methylene groups, stretching C≡C modes (2087 and 2115 cm^{-1}), and a stretching C=C mode (1515 cm^{-1}), whose presence results from the UV-induced polymerization process.

In order to control the growth of $(EDT\text{-}TTFVO)_4(FeCl_4)_2$, in particular to avoid the presence of randomly distributed single crystals, we have used a Si-supported multilamellar membrane as anode in the electrocrystallization of EDT-TTFVO in the presence of $[(n\text{-}C_2H_5)_4N]FeCl_4$ in chlorobenzene–ethanol as solvent mixture. Before electrodeposition, the Si-supported multilayer was incubated in the electrochemical cell for about 30 min to make the multilayer swell to the fully solvated state, *i.e.* the interheadgroup spaces are filled with ethanol (in which $[(n\text{-}C_2H_5)_4N]FeCl_4$ is very soluble) and the long-chain area with chlorobenzene and presumably a small amount of ethanol. In this solvent mixture, EDT-TTFVO is relatively soluble. The electrochemical oxidation was carried

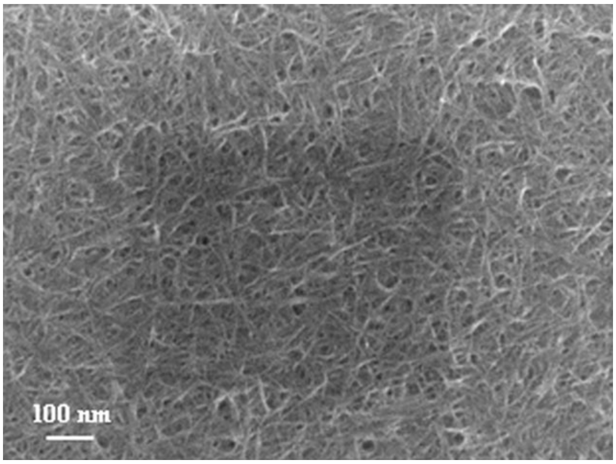

Fig. 10 SEM image of $(EDT\text{-}TTFVO)_4(FeCl_4)_2$ nanofibre films grown on Si-supported multilamellar membranes.

out for 10 days at 0.15 μA cm^{-2}, and a very thin black deposit was found to cover the membrane surface. Shorter-time electrolysis gave no deposit, whereas longer-time electrodeposition ($10 < t < 30$ days) leads to no significantly thicker deposits. Furthermore, using n-type silicon instead of intrinsic silicon and higher current densities give similar results as those described above.

Electron micrographs evidence that the film is actually made of severely aggregated nanofibres (diameter ≤20 nm, Fig. 10). Their Raman spectrum (Fig. 8, spectrum B) is almost identical to that obtained on $(EDT\text{-}TTFVO)_4(FeCl_4)_2$ single crystals. Bands at 261vw, 313vw, 501s, 747w, 1007w, 1415s, 1469sh and 1626br observed in the Raman spectrum of nanofibres have the same assignments as those for $(EDT\text{-}TTFVO)_4(FeCl_4)_2$ single crystals (*vide supra*). In this case, the nanofibre growth is not so surprising as in case of $Per_2[Au(mnt)_2]$. A plausible mechanism is conceivable as follows: EDT-TTFVO molecules migrate from the solution/membrane interface to the substrate surface *via* long alkyl chains, and are oxidized to produce the charge-transfer salt with $FeCl_4^-$ ions which are largely present at the proximity of the hydrophilic silicon surface. The salt growth gradually starts to occur. As the growing salt is in contact with $FeCl_4^-$ ions in interheadgroup spaces, the growth can continue to form nanofibres along free channels between the long alkyl chains. Even when the growing salt reaches the membrane surface, the growth still continues towards the formation of long nanofibres perpendicular to the membrane surface, as evidenced by scanning electron microscopy (Fig. 10). The preparation of thicker deposits or an alternative technique (such as the four-probe method) to enable measurements of transport properties of the nanofibres require to be done.

Conclusions

We have fabricated wire-shaped crystals of [TTF][TCNQ] using an adsorption in solution technique on stainless steel conversion coatings. Nanowires were well dispersed on the substrate and their transport properties have been evaluated after their removal from the surface. However, it is to be noted that such a technique, though easy to carry out, is not suitable when oxidation of the donor molecule is electrochemically induced, which is the most frequently encountered case. We have also been able to prepare nanowire films on a silicon wafer used as an anode, which constitutes a more "universal" technique. $Per_2[Au(mnt)_2]$ has been surprisingly grown as aggregated semiconducting nanowires on a conventional intrinsic Si wafer. The use of Si-supported multilamellar templates allowed fabrication of $(EDT\text{-}TTFVO)_4(FeCl_4)_2$ nanofibres. This technique appears to be the most suitable for preparing a large variety of molecule-based conductors exhibiting a nanowire-like morphology.

Acknowledgements

This work was supported by CNRS, in part under a CNRS/AIST programme. J.-P. S. thanks the Fond Social Européen (FSE) for a PhD grant and Université Paul Sabatier for ATUPS financial support. The authors gratefully thank Dr A. Zwick and Dr C. Routaboul for Raman measurements, and M. Reversat and V. Collière for SEM characterizations. Finally, D. Bérail from Motorola is acknowledged for supplying supports for the conductivity measurements.

References

1 *Inorganic Materials*, ed. D. W. Bruce and D. O'Hare, J. Wiley & Sons, Chichester, 1996, ch. 1, 2 and 3.
2 L. Valade, D. de Caro, M. Basso-Bert, I. Malfant, C. Faulmann, B. Garreau-de Bonneval and J.-P. Legros, *Coord. Chem. Rev.*, 2005, **249**, 1986.
3 J. Hossick Schott and M. D. Ward, *J. Am. Chem. Soc.*, 1994, **116**, 6806.
4 F. Favier, H. Liu and R. M. Penner, *Adv. Mater.*, 2001, **13**, 1567.
5 T. Akutagawa, T. Ohta, T. Hasegawa, T. Nakamura, C. A. Christensen and J. Becher, *Proc. Natl. Acad. Sci. U. S. A.*, 2002, **99**, 5028.
6 C. Colin, C. R. Pasquier, P. Auban-Senzier, F. Restagno, S. Baudron, P. Batail and J. Fraxedas, *Synth. Met.*, 2004, **146**, 273.
7 L. Valade, H. Casellas, S. Roques, C. Faulmann, D. de Caro, A. Zwick and L. Ariès, *J. Solid State Chem.*, 2002, **168**, 438.
8 G. Cui, W. Xu, C. Guo, X. Xiao, H. Xu, D. Zhang, L. Jiang and D. Zhu, *J. Phys. Chem. B*, 2004, **108**, 13638.
9 M. Sakai, M. Izuka, M. Nakamura and K. Kudo, *Jpn. J. Appl. Phys., Part 1*, 2003, **42**, 2488.
10 L.-L. Xing, D.-P. Li, S.-X. Hu, H.-Y. Jing, H. Fu, Z.-H. Mai and M. Li, *J. Am. Chem. Soc.*, 2006, **128**, 1749.
11 V. Rousset, C. Joachim, T. Ondarçuhu and B. Rousset, *Eur. Phys. J.*, 1998, **AP 3**, 21.
12 K. Yase and Y. Yoshida, *Jpn. J. Appl. Phys., Part 1*, 1995, **34**, 3903.
13 J. Caro, S. Garelik and A. Figueras, *Chem. Vap. Deposition*, 1996, **2**, 251.
14 J. Fraxedas, S. Molas, A. Figueras, I. Jiménez, R. Gago, P. Auban-Senzier and M. Goffman, *J. Solid State Chem.*, 2002, **168**, 384.
15 D. de Caro, J. Sakah, M. Basso-Bert, C. Faulmann, J.-P. Legros, T. Ondarçuhu, C. Joachim, L. Ariès, L. Valade and P. Cassoux, *C. R. Acad. Sci., Ser. IIc: Chim.*, 2000, **3**, 675.
16 L. Ariès and J.-P. Traverse, *Eur. Pat.*, EP 874000318, 1987.
17 L. Ariès, *J. Appl. Electrochem.*, 1994, **24**, 554.
18 H. Lui, Q. Zhao, Y. Li, F. Lu, J. Zhuang, S. Wang, L. Jiang, D. Zhu, D. Yu and L. Chi, *J. Am. Chem. Soc.*, 2005, **127**, 1120.
19 S. Matsuzaki, M. Onomichi, H. Tomura, S. Yoshida and K. Toyoda, *Mol. Cryst. Liq. Cryst.*, 1985, **120**, 93.
20 R. Bozio, I. Zanon, A. Girlando and C. Pecile, *J. Chem. Phys.*, 1979, **71**, 2282.
21 A. Graja, *Spectroscopy of Materials for Molecular Electronics*, Scientific Publishers OWN, Poznan, 1997.

22 Z. Z. Wang, J.-C. Girard, C. Pasquier and D. Jérome, *J. Phys. IV*, 2003, **114**, 91.
23 J. Voit, F. Zwick, D. Jérome, G. Margaritondo, M. Onellion and M. Grioni, *Phys. Rev. Lett.*, 1998, **81**, 2974.
24 D. de Caro, J. Fraxedas, C. Faulmann, I. Malfant, J. Milon, J.-F. Lamère, V. Collière and L. Valade, *Adv. Mater.*, 2004, **16**, 835.
25 D. de Caro, H. Alves, M. Almeida, S. Cailleux, M. Elgaddari, C. Faulmann, I. Malfant, F. Senocq, J. Fraxedas, A. Zwick and L. Valade, *J. Mater. Chem.*, 2004, **14**, 2801.
26 A. Kowalska, J.-P. Savy, D. de Caro, C. Faulmann, L. Valade and J. Ulanski, *J. Mol. Struct.*, 2006, **792–793**, 146.
27 I. Malfant, K. Rivasseau, J. Fraxedas, C. Faulmann, D. de Caro, L. Valade, L. Kaboub, J.-M. Fabre and F. Senocq, *J. Am. Chem. Soc.*, 2006, **128**, 5612.
28 T. Nakamura, Y. Miura, M. Matsumoto, H. Tashibana, M. Tanaka and Y. Kawabata, in *The Physics and Chemistry of Organic Superconductors*, ed. G. Saito and S. Kagoshima, Springer Proceedings in Physics, Springer-Verlag, Berlin/Heidelberg, 1990, vol. 51, pp. 424.
29 M. Almeida and R. T. Henriques, in *Handbook of Organic Conductive Molecules and Polymers*, ed. Hari Singh Nalwa, J. Wiley & Sons, Chichester, 1997, vol. 1, pp. 87.
30 E. B. Lopes, M. J. Matos, R. T. Henriques, M. Almeida and J. Dumas, *Phys. Rev. B: Condens. Matter*, 1995, **52**, R2237.
31 D. Graf, J. S. Brooks, E. S. Choi, S. Uji, J. C. Dias, M. Almeida and M. J. Matos, *Phys. Rev. B: Condens. Matter*, 2004, **69**, 125113.
32 H. L. Liu, D. B. Tanner, A. E. Pullen, K. A. Abboud and J. R. Reynolds, *Phys. Rev. B: Condens. Matter*, 1996, **53**, 10557.
33 M. K. Johnson, Dithiolene Chemistry Synthesis, Properties, and Applications, *Prog. Inorg. Chem.*, 2004, **52**, 213.
34 S.-G. Liu, P.-J. Wu, Y. Q. Liu and D.-B. Zhu, *Mol. Cryst. Liq. Cryst.*, 1996, **275**, 211.
35 H. H. Wang, K. L. Stamm, J. P. Parakka and C. Y. Han, *Adv. Mater.*, 2002, **14**, 1193.
36 R. Shen, W. Xu, D. Zhang and D. Zhu, *Solid State Commun.*, 2004, **130**, 401.
37 L. Valade, D. de Caro, J.-P. Savy, I. Malfant, C. Faulmann, M. Almeida J. Fraxedas and J. S. Brooks, *J. Low Temp. Phys.*, 2006, **142**, 393.
38 L. Valade, J. Fraxedas, D. de Caro, J.-P. Savy, I. Malfant, C. Faulmann and M. Almeida, *J. Low Temp. Phys.*, 2006, **142**, 141.
39 J. J. Pireaux, M. Liehr, P. A. Thiry, J. P. Delrue and R. Caudano, *Surf. Sci.*, 1984, **141**, 221, and references therein.
40 E. Ojima, H. Fujiwara, K. Kato, H. Kobayashi, H. Tanaka, A. Kobayashi, M. Tokumoto and P. Cassoux, *J. Am. Chem. Soc.*, 1999, **121**, 5581.
41 H. Fujiwara, E. Fujiwara, Y. Nakazawa, B. Z. Narymbetov, K. Kato, H. Kobayashi, A. Kobayashi, M. Tokumoto and P. Cassoux, *J. Am. Chem. Soc.*, 2001, **123**, 306.
42 S. Uji, H. Shinagawa, T. Terashima, T. Yakabe, Y. Terai, M. Tokumoto, A. Kobayashi, H. Tanaka and H. Kobayashi, *Nature*, 2001, **410**, 908.
43 T. Matsumoto, T. Kominami, K. Ueda, T. Sugimoto, T. Tada, H. Yoshino, K. Murata, M. Shiro, E. Negishi, H. Matsui, N. Toyota, S. Endo and K. Takahashi, *J. Solid State Chem.*, 2002, **168**, 408.
44 T. Matsumoto, T. Kominami, K. Ueda, T. Sugimoto, T. Tada, S. Noguchi, H. Yoshino, K. Murata, M. Shiro, E. Negishi, N. Toyota, S. Endo and K. Takahashi, *Inorg. Chem.*, 2002, **41**, 4763.
45 T. Matsumoto, T. Sugimoto, H. Aruga Katori, S. Noguchi and T. Ishida, *Inorg. Chem.*, 2004, **43**, 3780.
46 M. Wang, H. Fujiwara, T. Sugimoto, S. Noguchi and T. Ishida, *Inorg. Chem.*, 2005, **44**, 1184.
47 T. Hiraoka, Y. Kamada, T. Matsumoto, H. Fujiwara, T. Sugimoto, S. Noguchi, T. Ishida, H. Nakazumi and H. Aruga Katori, *J. Mater. Chem.*, 2005, **15**, 3479.
48 G. P. Bhavsar and K. Sathianandan, *J. Mol. Struct.*, 1973, **16**, 343.
49 M. E. Kozlov, K. I. Pokhodnia and A. A. Yurchenko, *Spectrochim. Acta, Part A*, 1987, **43**, 323.